28 October 1994

ELSEVIER

Chemical Physics Letters 229 (1994) 211–217

CHEMICAL PHYSICS LETTERS

Intensity effects on impulsive excitation of ground surface coherent vibrational motion. A 'V' jump simulation

Allon Bartana, Uri Banin, Sanford Ruhman, Ronnie Kosloff

Department of Physical Chemistry and the Fritz Haber and Farkas Research Centers, the Hebrew University, Jerusalem 91904, Israel

Received 3 August 1994

Abstract

Control of coherent ground surface dynamics is achieved by varying the intensity of a resonant ultrafast pump pulse. This pulse cycles amplitude between the ground and excited electronic surfaces resulting in a momentum kick and a coordinate dependent loss of amplitude, creating a nonstationary vibrational distribution: the 'V' jump. A qualitative change in composition occurs for intensities above π pulse conditions. The induced dynamics is observed by a delayed pulse which is dispersed and analyzed against time or as a two-dimensional frequency plot. Such an analysis makes it possible to distinguish the contributions of high vibrational harmonics to the dynamics.

1. Introduction

The purpose of this Letter is to demonstrate, by example, the use of excitation pulse intensity in the control of impulsively induced ground surface vibrational dynamics. The demonstration is based on the dynamics of the symmetric stretch mode of the I_3^- molecule ion which has been the subject of experimental [1] and theoretical study [2]. Upon excitation by an ultrashort pulse, amplitude from the ground surface is transferred to the dissociative excited surface. The combination of the loss of amplitude from the ground surface and of amplitude cycling with the excited surface leads to a dynamical 'hole' in the ground surface density. The creation of the dynamical 'hole' can be considered as a 'V' jump experiment in analogy to the 'T' jump experiment, where a nonstationary distribution is created abruptly and then is followed by a delayed probe. This nonstationary 'hole' then interrogates the ground surface dynamics. The main result of this simulation is the marked difference both in the shape of the dynamical 'hole' and in the transient spectroscopy which accompanies it upon increasing the pump fluence.

2. The model

A nonperturbative treatment of the light matter interaction is the basis of the model. The model addresses a molecule with a bound ground surface and a dissociative excited surface. In a wave packet picture the state of the system is described by the vector

$$\psi = \begin{pmatrix} \psi_e \\ \psi_g \end{pmatrix}. \tag{1}$$

The dynamics, including the excitation field, is generated by the Hamiltonian

$$\hat{H} = \hat{H}_0 + \hat{V}_t, \tag{2}$$

where

$$\hat{\mathbf{H}}_0 = \begin{pmatrix} \hat{\mathbf{H}}_e & 0 \\ 0 & \hat{\mathbf{H}}_g \end{pmatrix}$$

and

$$\hat{\mathbf{V}}_t = \hat{\mathbf{V}}_t(t) = \begin{pmatrix} 0 & -\epsilon\hat{\mu} \\ -\epsilon^*\hat{\mu} & 0 \end{pmatrix}, \tag{3}$$

where $\epsilon = \epsilon(t) = \bar{\epsilon}(t)\, e^{-i\omega t}$ is the time dependent field and $\hat{\mu}$ the dipole operator. $\hat{\mathbf{H}}_{g/e}$ are the surface Hamiltonians: $\hat{\mathbf{H}}_l = \hat{\mathbf{P}}^2/2M + \hat{\mathbf{V}}_l$.

The influence of a short impulsive pulse is examined next. In particular a pulse duration is used in which the nuclear motion is almost frozen but is long on the time-scale of electronic transition. The model is based on the symmetric stretch mode of I_3^- which eventually photodissociates on the excited surface to $I_2^- + I$ [1]. (Table 1 summarizes the potential energy description.) For this system the impulsive duration is between 10 and 30 fs compared to a vibrational period of 300 fs and to an electronic transition period of $1/\omega$ of 1 fs. Under these conditions the ground surface wavefunction immediately after the pulse ($t = t_f$), is approximated by using a coordinate dependent two-level system [2,3]. This leads to

$$\psi_g(\boldsymbol{r}, t_f) = \exp[-(i/\hbar)E_g t_f] \exp[-(i/\hbar)\Delta t_f] \times [\cos(\Omega t_f) + i\cos\theta \sin(\Omega t_f)]\psi_g(\boldsymbol{r}, 0), \tag{4}$$

where $\Omega(\boldsymbol{r}) = (1/\hbar)\sqrt{W^2 + \Delta(\boldsymbol{r})^2}$ is the coordinate dependent Rabi frequency which depends on the field intensity $\bar{\epsilon}$: $W \approx \bar{\epsilon}\mu(\boldsymbol{r})$ ($\bar{\epsilon}$ is the slowly varying field envelope in the RWA picture), and $\hat{\Delta}(\boldsymbol{r})$ is the coordinate-dependent detuning value $2\hat{\Delta} = \hat{\mathbf{V}}_e(\boldsymbol{r}) - \hat{\mathbf{V}}_g(\boldsymbol{r})$. The angle θ in Eq. (4) is defined by

$$\cos\theta = \frac{|\Delta|}{\sqrt{W^2 + \Delta^2}}. \tag{5}$$

Examining Eq. (4) it is noticed that at the point of resonance ($\Delta(\boldsymbol{r}) = 0$), $\cos\theta = 0$ therefore $\psi_g(\boldsymbol{r}_{res}) \propto \cos(Wt_f)$. For the conditions where $2Wt_f = \pi$, all amplitude at the point of resonance is transferred to the excited surface. This will be termed a π pulse. For all other internuclear distances the detuning is nonzero. Therefore the Rabi frequency $\Omega(\boldsymbol{r})$ becomes higher and more cycling occurs. However less amplitude is transferred since $\cos^2\theta < 1$. This coordinate dependent cycling leads to a local phase change in the wavefunction. A coordinate dependent phase is equivalent to a momentum shift. Fig. 1 shows the wavepacket after the pulse. It has been directly calculated by a numerical solution of the time-dependent Schrödinger equation. For the pulse durations that were used to generate the figure the exact calculation is indistinguishable from Eq. (4) (see Table 1 for details).

The Rabi cycling at resonance can go beyond the π pulse conditions. By increasing the intensity so that $2Wt_f = 2\bar{\epsilon}\mu t_f = 2\pi$, a full cycle occurs and the amplitude returns to the ground surface at the point of perfect resonance. The effect of this 2π pulse on the wavefunction is also shown in Fig. 1. The increase in

Table 1
Typical parameters of propagation

potential ground surface:	$v_g = \frac{1}{2}M\omega_v^2(r - r_{eq})^2$, $\omega_v = 112.0\ cm^{-1}$, $M = \frac{1}{2}127$ amu, $r_{eq} = 2.95$ Å		
potential excited surface:	$V_e(r) = D\exp[-\beta(r - r_e)] + V_\infty$, $D = 0.7$ eV, $\beta = 3\ Å^{-1}$, $r_e = 2.95$ Å, $V_\infty = 3.55$ eV		
dipole function:	$\mu = a$, $a = 3.7$ au		
Propagation			
grid	$\Delta x = 1.92 \times 10^{-2}$	$N_x = 128$	$X_{min} = 2.3$ Å
mass	$m = \frac{1}{2}127$ amu		
	$\Delta t = 100$ au	$N_t = 100$	order = 64
field	$\epsilon(t) = \bar{\epsilon}\exp[-(2\ln 2/\tau^2)(t - t_0)^2]\exp(-i\omega_0)$		$\omega_0 = \hbar c/\lambda$
pump field	$\bar{\epsilon} = 1.25 \times 10^{-4}$ au	$\tau = 15$ fs	$\lambda = 292$ nm
probe field	$\bar{\epsilon} = 2.5 \times 10^{-5}$ au	$\tau = 15$ fs	$\lambda = 308$ nm
dispersed probe	$\bar{\epsilon} = 2.5 \times 10^{-5}$ au	$\tau = 6$ fs	$\lambda = 308$ nm

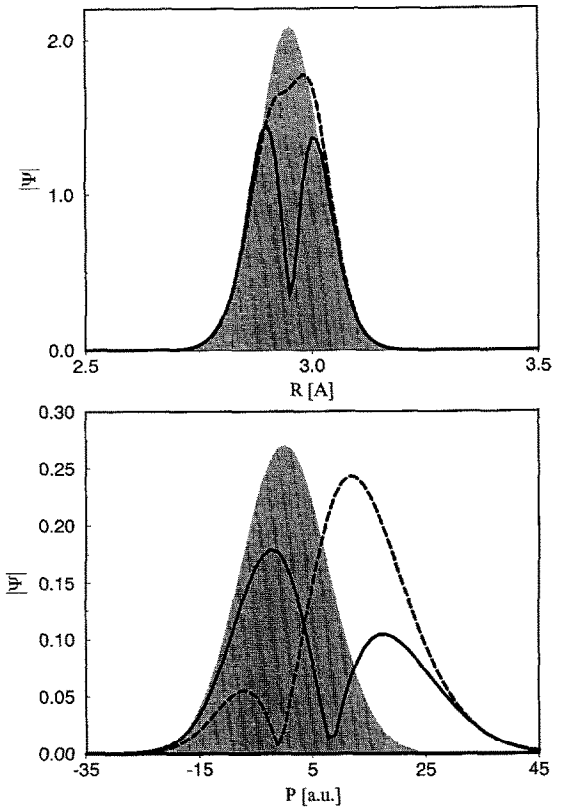

Fig. 1. The absolute value of the wavefunction before (gray) and after the pulse. Solid line is the π pulse wavefunction, and the dashed line the 2π pulse wavefunction. (The figure shows the wavefunction at a delay time of one vibrational period relative to the center of the pump pulse.) The upper panel displays the position distribution and the lower panel displays the momentum distribution. A 15 fs pulse was used with central frequency of 292 nm. The system models the symmetric stretch mode of I_3^- for $v=0$.

cycling also results in a larger momentum shift shown in the momentum distribution in Fig. 1. In comparison the π pulse has a smaller average momentum.

The excitation pulse creates a nonstationary distribution out of the equilibrium stationary one. Thus it is advantageous to decompose the state after the excitation pump pulse into its dynamical and static contributions [2],

$$\hat{\rho}(t_f)=\hat{\rho}_d+c^2\hat{\rho}_s\,, \tag{6}$$

where $\hat{\rho}(t_f)$ is the density operator of the system after the pulse, and $\hat{\rho}_s$ is the stationary component constituted from the diagonal elements of $\hat{\rho}$ in the energy representation [2]. The dynamical contribution $\hat{\rho}_d$ is

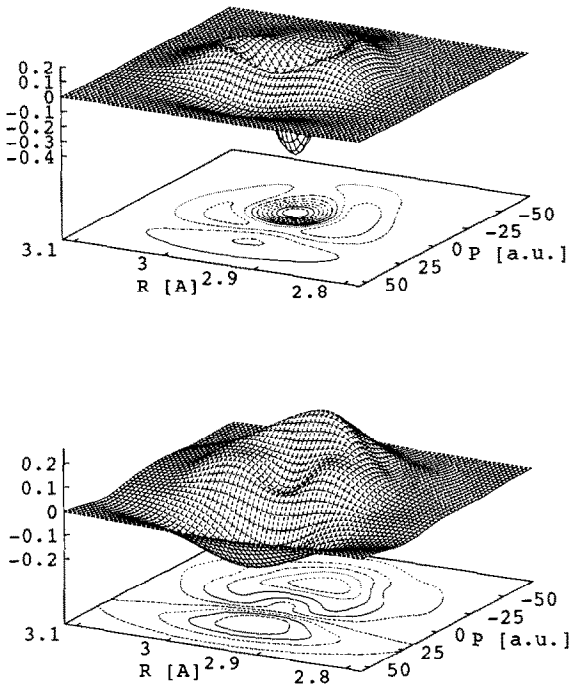

Fig. 2. A phase-space Wigner distribution function of the dynamical hole created by a 15 fs pump pulse from a thermal distribution of 300 K. Upper panel shows a π pulse distribution and the lower panel shows a 2π pulse distribution.

the rigorous definition of the dynamical 'hole' and is therefore responsible for the experimental probe pulse signal. Fig. 2 shows the phase space projection of the dynamical 'hole' for the π and 2π pulses, with a thermal initial state. It can be seen that compared to the π pulse case the 2π distribution is very different, the π pulse possesses a more peaked distribution. The shape of the weak pulse 'hole' (not shown) resembles the general shape of the π pulse 'hole'.

3. Probing the dynamics

The large difference in the shape of the dynamical 'hole' generated by pulses with different intensities is reflected by the probe signal. The simplest approach is to monitor the total absorption of the probe pulse. The signal can be calculated under the RWA conditions to all orders in the field, from the total change of normalization on the ground surface induced by the probe pulse:

$$\Delta E(t_d) = \int_{t_d - \tau_{pr}/2}^{t_d + \tau_{pr}/2} \mathscr{P}(t')\,dt' = -\hbar\omega\Delta N_g, \qquad (7)$$

where t_d is the pump probe delay time, τ_{pr} is the probe pulse duration, $\mathscr{P}(t)$ the power absorbed from the field and ΔN_g is the normalization change on the ground surface [2,4].

Fig. 3 shows the absorption signal as a function of the time delay between pump and probe for a weak (linear), π and 2π pulses. To emphasize the difference in the dynamics created by these two pulses the Fourier transform of the signal is also shown in Fig. 3. The amplitude of the signal reflects the intensity. The harmonic components of the signal are very different. The linear and π pulse have an enhanced second harmonic signal relative to the 2π pulse. Other harmonics show different variations. The enhancement of the second harmonic can be reversed if the pump pulse is tuned to the edge of the absorption band.

An impulsive probe pulse has a broad spectral range, therefore a more informative probe is obtained, if after the pulse propagates through the medium it is dispersed. Then the dispersed spectrum is compared to the spectrum of a reference pulse [5–7]. In order to relate the observation to a molecular property, the absorbed power is integrated and the integration limits are changed from $-\infty$ to ∞. The total amount of energy absorbed from the field becomes

$$\Delta E_f \approx \int_{-\infty}^{\infty} \mathscr{P}\,dt$$

$$= 2\,\mathrm{Real}\left(\int_{-\infty}^{\infty} \langle \hat{\mu}\otimes\hat{S}_+ \rangle \cdot \frac{\partial \epsilon}{\partial t}\,dt\right). \qquad (8)$$

For a single component wavefunction, the induced polarization $\langle \hat{\mu}\otimes\hat{S}_+ \rangle = \langle \psi_e | \mu | \psi_g \rangle$. For a thermal distribution this quantity is averaged with Boltzmann weights. Defining the Fourier transform of the instantaneous dipole expectation,

$$\langle \hat{\mu}\otimes\hat{S}_+ \rangle(\omega) = \int_{-\infty}^{\infty} \langle \hat{\mu}\otimes\hat{S}_+ \rangle(t)\, e^{i\omega t}\,dt. \qquad (9)$$

Using the Fourier transform of the field $\epsilon(\omega)$, the energy absorption from a thin sample can be written as [8]

$$\Delta E_f = -2\,\mathrm{Real}\left(\int_{-\infty}^{\infty} i\omega \langle \hat{\mu}\otimes\hat{S}_+ \rangle(\omega)\cdot\epsilon^*(\omega)\,d\omega\right). \qquad (10)$$

This suggests the decomposition of energy to frequency components, $\Delta E_f = \int_{-\infty}^{\infty} \Delta E_f(\omega)\,d\omega$. Normalizing each frequency component to the energy density of the pulse leads to the expression

$$\sigma_a(\omega, t_d) = \frac{\Delta E_f(\omega)}{|\epsilon(\omega)|^2}$$

$$= -2\omega\,\mathrm{Imag}\left(\frac{\langle \hat{\mu}\otimes\hat{S}_+ \rangle(\omega)}{\epsilon(\omega)}\right). \qquad (11)$$

This expression resembles the one presented by Pollard and Mathies [5] and Yan and Mukamel [9] but since its derivation is not based on a perturbation expansion, it is correct for strong fields (see also Ref. [10]). Fig. 4 compares the dispersed signal as a function of the time delay for dynamics induced by a π

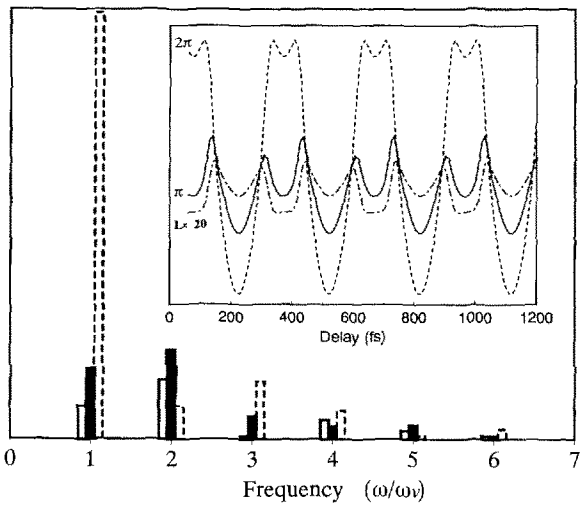

Fig. 3. The total energy absorbed from a 15 fs probe pulse as a function of time delay between pump and probe (insert), and its Fourier transform for different pulse intensities, for the same conditions of Fig. 2. The linear $\pi/8$ pulse signal is multiplied by 20 shown as a dashed dot line and the first empty histogram in the Fourier plot. The π pulse is displayed as a solid line and the second solid histogram and 2π pulse is displayed as a dashed line and the third dashed histogram.

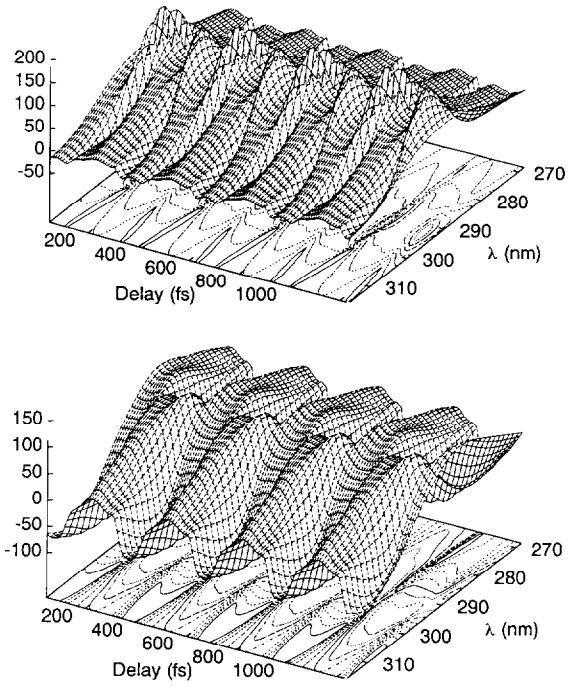

Fig. 4. The dispersed probe absorption signal as a function of time delay between pump and probe and wavelength. Upper panel π pulse, lower panel 2π pulse. The initial conditions are the same as Fig. 2 with a 6 fs probe pulse.

and 2π pulses. Examining the signals it is apparent that each are different from the other. Nevertheless it is difficult to interpret the signal in terms of its specific dynamics.

To facilitate the interpretation the signal $\sigma_a(\omega, t_d)$ is Fourier transformed to

$$\sigma_a(\omega, \Omega) = \int_0^\infty \sigma_a(\omega, t)\, e^{-i\Omega t}\, dt\,, \qquad (12)$$

resulting in the two-dimensional frequency plot shown in Fig. 5. From Fig. 5, it can be seen that different harmonics of the vibrational motion can be correlated to the probe dispersed frequency ω.

4. Discussion

Ultrafast pump–probe experiments have become established in the study of molecular dynamics

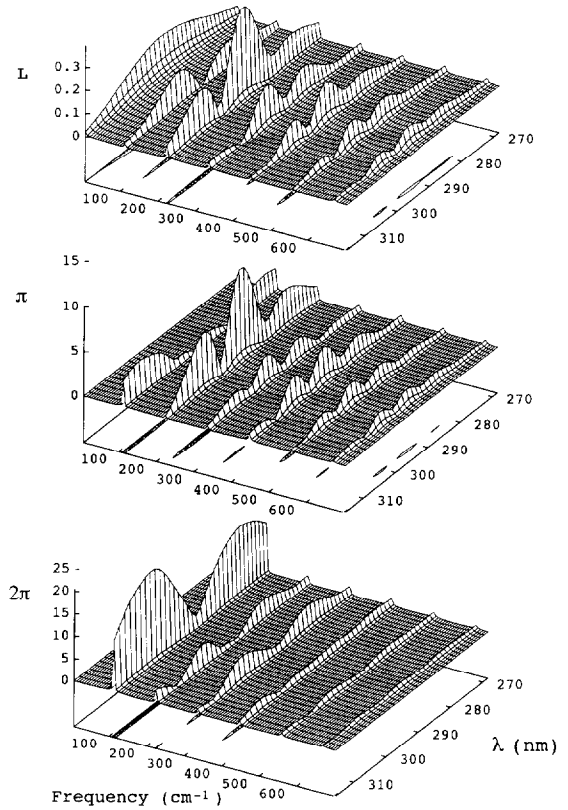

Fig. 5. A two-dimensional frequency plot of the dispersed probe absorption signal obtained by a Fourier transform of the time axis of Fig. 4. The cm^{-1} frequency scale corresponds to the vibrational overtone frequency range. Upper panel linear pulse, middle panel π pulse, lower panel 2π pulse.

[11,12]. The appealing aspect of the method is that the pump pulse can set in motion a specific type of dynamical event which is then followed in a causal fashion by the probe pulse. In this study, the intensity of the excitation pulse becomes a control on the impulsively induced ground surface dynamics. This control is in line with other work which has the objective of controlling the energy content of a specific degree of freedom [13–15]. In the study of condensed phase dynamics the intensity control which is able to create large amplitude motion, allows a channel to understand the mechanism of the disposal of large quantities of vibrational energy in the stabilization of exothermic reactions.

Another advantage of this method over other schemes is that it is relatively easy to perform. The usefulness of the control depends on the ability to in-

terpret the experimental consequences in terms of the underlying dynamics. The common method of interpretation of ultrafast pump–probe experiments is based on a perturbative expansion in the field intensity [5–7,9,16–19] and is obviously inappropriate. Therefore a nonperturbative method is employed. The central object in the method is the dynamical 'hole' which carrying all the transient information. By using the concept of the coordinate dependent two-level system the creation of the 'hole' can be rationalized in terms of the frequency, intensity and duration of the excitation pulse.

The approach is valid for a pulse duration which is shorter than any induced nuclear motion. For example for I_3^-, pulses of 60 fs which are still able to promote coherent motion are not impulsive enough. The nuclear motion during the pulse effectively increases the linear region where Rabi cycling is not important. The impulsive limit for this molecule is below 30 fs. The use of high-intensity pulses may cause undesired side effects. Specifically for the I_3^- system to check for possible complications, the peak intensity for a π pulse is calculated to be 6.6×10^{10} W/cm^2 which is still below the limit of white light generation of the solvent, meaning the pulse intensity is still within manageable limits.

In the impulsive limit the two main control levels on the induced ground surface dynamics are the frequency and intensity of the excitation pulse. A trivial but important aspect of the pulse intensity is that the amplitude of the signal linearly increases with the pulse fluence. The dependence of the shape or relative composition of the dynamical 'hole' on intensity is more subtle. Based on many simulations where the excitation frequency was varied, the shape of the dynamical 'hole' stays relatively constant from weak intensities up to intensities close to π pulse conditions. Up to this fluence, the dynamical 'hole' consists mainly of missing amplitude lost to the excited surface close to the point of resonance. This can be seen in Figs. 3 and 5 where the relative ratios of the contribution of the first and second harmonic of the linear and π pulse signals are similar. For intensities above π pulse conditions the shape of the dynamical 'hole' changes significantly due to amplitude cycling leading to a momentum kick.

For pulses detuned to the red or blue of the middle of the absorption band, one observes a rotation of the dynamical 'hole' in phase space by 90°, when the intensity is raised from π to 2π conditions. This rotation reflects the intensity controlled transition from position to momentum erosion.

For excitation pulses in the middle of the band which created the distributions shown in Figs. 1 and 2, the difference is more subtle. For weak to π pulses the 'hole' which is in the middle of the position distribution enhances the second harmonic signal [20]; this effect is observed in Figs. 3 and 5. The harmonics which show up prominently in the spectral modulation reflect the angular moments of the dynamical 'hole' which have been most drastically influenced by the pump excitation. The variation from a weak excitation to the π pulse has also induced a phase shift of 180° in the spectral modulations at the fundamental frequency (Fig. 3). The 2π pulse refills the 'hole' in position and therefore the second harmonic signal is very much depressed. Nonetheless the substantial control provided by the intensity on the shape of the dynamical 'hole' is apparent in this case also.

Once the 'hole' is created, it is subject to ground surface dynamics. For experiments conducted in condensed matter, dissipative dynamics have to be used. Solution of the Liouville–Von Neumann equation including the light–matter interaction with dissipation can be performed [2]. The dissipation increases the Rabi frequency but will reduce the amount of transferred amplitude. In these calculations only thermal averaging was considered. For room-temperature experiments the thermal averaging only slightly reduces the total signal. This is also expected considering averaging due to different initial orientations.

The analysis of the ground surface dynamics can be perturbed by dynamics on the excited surface. The problem is enhanced if the excited surface is bound which will make it difficult to distinguish between the ground and excited surface dynamics. Such a complication can be reduced by using a 2π excitation pulse since it minimizes the amplitude transfer to the excited surface but generates a large amplitude motion on the ground surface.

The dynamics experienced by the 'hole' can be detected in various ways. Pollard et al. [5,6] have analyzed a probe based on the dispersion of a delayed short pulse. Their derivation uses a perturbation series in the field intensity to calculate the observed sig-

nal. This study extends the calculation of the signal for high intensities. It is significant since it has been shown by Ebel and Schinke [21] that even for 3% convergence, substantial deviations are obtained between the perturbative signal and the nonperturbative one.

The drawback of the dispersed signal picture (Fig. 4) is that its underlying vibrational dynamics are difficult to interpret. To facilitate the interpretation, a two-dimensional frequency plot (Fig. 5) has been constructed. This plot allows the dynamics to be unraveled in terms of the vibrational harmonics of the motion. This two-dimensional frequency plot is different from the optical analogue [22] of the two-dimensional NMR spectroscopy [23]. The two-dimensional spectroscopy employs a train of three pulses whereas in this case the dispersion of the short probe pulse supplies one of frequency scales.

Considering laser selective chemistry, one has in mind an ultimate final goal of enhancement of a specific chemical species [24]. In this study the control achieved by varying the intensity and frequency has a more limited objective, of shaping the ground surface dynamical 'hole'. This objective is similar in spirit to laser cooling of vibrational motion [14]. Nevertheless control of the ground surface dynamics can lead eventually to the control of chemical significance. For example in the Na_2 system, two possible ionized products exist. The intensity of the pulses has been used to control the relative yield of the two possible products [25].

In conclusion, this study points to the expected benefits of using the intensity of a pulse as a control in an ultrafast pump–probe experiment. However many complications have been overlooked. They will require more experimental and theoretical analysis.

Acknowledgement

This research has been supported by the Binational United States–Israel Science Foundation and the Israel Science Foundation. The Farkas and the Fritz Haber Research Centers are supported by the Minerva Gesellschaft für die Forschung, GmbH München, FRG.

References

[1] U. Banin, A. Waldman and S. Ruhman, J. Chem. Phys. 96 (1992) 2416;
U. Banin and S. Ruhman, J. Chem. Phys. 98 (1993) 4391;
U. Banin, R. Kosloff and S. Ruhman, Isr. J. Chem. 33 (1993) 141.
[2] U. Banin, A. Bartana, S. Ruhman and R. Kosloff, J. Chem. Phys. (1994), submitted.
[3] K.-A. Suominen, B.M. Garraway and S. Stenholm, Phys. Rev. A 45 (1992) 3060.
[4] A. Dell Hammerich, R. Kosloff and M. Ratner, J. Chem. Phys. 97 (1992) 6410.
[5] W.T. Pollard and R.A. Mathies, Ann. Rev. Phys. Chem. 43 (1992) 497.
[6] W.T. Pollard, S.L. Dexheimer, Q. Wang, L.A. Peteanu, C.V. Shank and R.A. Mathies, J. Phys. Chem. 96 (1992) 6147.
[7] S.L. Dexheimer, Q. Wang, L.A. Peteanu, W.T. Pollard, R.A. Mathies and C.V. Shank, Chem. Phys. Letters 188 (1992) 61.
[8] J.D. Jackson, Classical electrodynamics (Wiley, New York, 1975) pp. 624, 802.
[9] Y.J. Yan and S. Mukamel, Phys. Rev. A 41 (1990) 6485.
[10] G. Ebel and R. Schinke, J. Chem. Phys. 101 (1994), in press.
[11] L.R. Khundkar and A.H. Zewail, Ann. Rev. Phys. Chem. 41 (1990) 15;
A.H. Zewail, Faraday Discussions Chem. Soc. 91 (1991) 207.
[12] M. Gruebele and A.H. Zewail, J. Chem. Phys. 98 (1993) 883;
M.J. Rosker, M. Dantus and A.H. Zewail, J. Chem. Phys. 89 (1988) 6113.
[13] R. Kosloff, A.D. Hammerich and D.J. Tannor, Phys. Rev. Letters 69 (1992) 2172.
[14] A. Bartana, R. Kosloff and D.J. Tannor, J. Chem. Phys. 99 (1993) 196.
[15] J.A. Cina and T.J. Smith, J. Chem. Phys. 98 (1993) 9211.
[16] J.S. Meslinger and Albrecht, J. Chem. Phys. 84 (1986) 1247.
[17] J. Chesnoi and A. Mokhtari, Phys. Rev. A 38 (1988) 3566.
[18] G. Stock and W. Domcke, J. Opt. Soc. Am. B 7 (1990) 1971.
[19] S. Mukamel, Ann. Rev. Phys. Chem. 41 (1990) 647.
[20] D.M. Jonas, S.E. Bradforth, S.A. Passimo and G. Fleming, Proc. Royal Dutch Academy Colloquium on Femtosecond Reaction Dynamics (Elsevier, Amsterdam, 1993).
[21] G. Ebel and R. Schinke, to be published.
[22] Y. Tanimura and S. Mukamel, J. Chem. Phys. 99 (1993) 9496.
[23] R.R. Ernst, G. Bodenhausen and A. Wokaum, Principles of nuclear magnetic resonance in one and two dimensions (Clarendon Press, Oxford, 1987).
[24] S.A. Rice, Science 258 (1992) 412;
D. Tannor and S.A. Rice, J. Chem. Phys. 83 (1985) 5013;
D. Tannor, R. Kosloff and S.A. Rice, J. Chem. Phys. 85 (1986) 5805.
[25] T. Baumet, R. Thalweiser, V. Weiss and G. Gerber, Femtosecond chemistry, eds. J. Manz and L. Wöste (Verlag Chemie, Weinheim, 1994).